Macromolecules
Cite This: Macromolecules 2019, 52, 5255−5267
Article
pubs.acs.org/Macromolecules

Deconvolution of the Effects of Binary Associations and Collective Assemblies on the Rheological Properties of Entangled Side-Chain Supramolecular Polymer Networks

Mostafa Ahmadi,*[,†,‡] Amir Jangizehi,[‡,§] Evelyne van Ruymbeke,*[,∥] and Sebastian Seiffert*[,‡]

[†]Department of Polymer Engineering and Color Technology, Amirkabir University of Technology, 15875-4413 Tehran, Iran
[‡]Institute of Physical Chemistry, Johannes Gutenberg-Universität Mainz, Duesbergweg 10-14, D-55128 Mainz, Germany
[§]Institute for Chemical Technology and Polymer Chemistry, Karlsruhe Institute of Technology (KIT), Engesserstraße 18, D-76131 Karlsruhe, Germany
[∥]Bio and Soft Matter, Institute of Condensed Matter and Nanosciences, Université Catholique de Louvain, Croix du Sud 1, B-1348 Louvain-la-Neuve, Belgium

Supporting Information

ABSTRACT: The properties and function of supramolecular polymer networks are determined not only by pairwise interchain transient associations but also by chain entanglement and nanoscopic phase separation of the associative groups. To unravel the impact and interplay of these different factors, we devise a set of model supramolecular polymer networks in which the number of entanglements and the density of associative groups are systematically varied. Rheological data show that by increasing the density of associative groups, the plateau modulus grows to a steady level and extends over a distinct frequency range. This is credited to the presence of binary associations with unique partner exchange time. For samples where the high-frequency plateau stays at the constant level, a second plateau emerges at low frequencies in addition. This plateau, which is well below the entanglement plateau of the precursor, is attributed to the presence of collective assemblies of nanophase-separated associative groups, as confirmed by FTIR spectroscopy. The contributions of these two different levels of interchain associations are decoupled on the basis of a tube-based model. The obtained model parameters show that by increasing the number of network junctions, including both interchain associations and entanglements, the fraction of binary associations decreases, while the density of collective ones approaches a constant level.

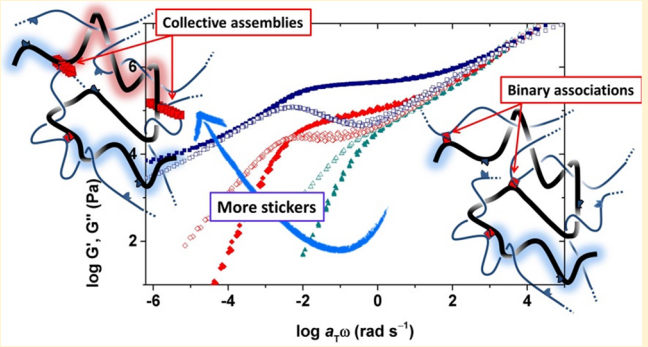

I. INTRODUCTION

Supramolecular polymer networks are frequently idealized by oligomeric or polymeric precursors that are physically cross-linked through transient reversible bonds.[1] The wide range of applicable physical bonds such as hydrogen bonding or metal−ligand coordination provides great versatility for tuning the dynamic and static mechanical properties of such systems.[2] Moreover, the strength of the physical bonds can be tailored by environmental conditions such as temperature or pH, which provides abilities for self-healing and stimuli responsiveness.[3,4] Therefore, these materials have found sophisticated applications in fields from drug delivery to catalysis and sensing.[5,6] However, in reality, such an ideal network is rarely encountered, and the overall behavior is significantly affected by several uncontrolled parameters. Namely, the dynamics of the entangled polymer precursor plays an important role, specifically at large chain length polydispersities.[7−10] Moreover, due to the difference in the polarity of the supramolecular associative motifs (often referred to as "stickers") and the polymer backbone or other long-range interactions such as $\pi-\pi$ stacking, associative groups are repeatedly reported to nano or microphase separate into ill-defined aggregates, clusters, or collective assemblies.[11−13] Such deviations from the idealized microstructural picture significantly alter the resulting properties of supramolecular polymer networks and therefore need to be defined and controlled to deliver the targeted functions.

Supramolecular polymer network systems can be classified into "main-chain" and "side-chain" type. In the first, associative moieties are located as terminal units of linear, star-shaped, or branched polymer precursors; in the second, such groups are located as pendants along the precursor polymer backbones. The rheological behavior of both types of supramolecular polymer networks can be explained in the light of tube-based models,[14−18] thereby providing the basis for rational material

Received: February 14, 2019
Revised: June 24, 2019
Published: July 9, 2019

DOI: 10.1021/acs.macromol.9b00323
Macromolecules 2019, 52, 5255−5267

design.[19−23] Based on the abovementioned classification, two different classes of tube-based models have been developed for main-chain and side-chain supramolecular polymer networks.[24,25]

Modeling the rheological properties of main-chain telechelic supramolecular polymer systems is challenging as the structure of the polymeric units changes dynamically in the course of stress relaxation. The attempt to combine such a random interconversion process with hierarchical relaxation mechanisms necessitates a robust stochastic model that is computationally expensive. In a seminal work, Cates included a dynamic random reversible scission of polymeric chains in a one-dimensional diffusion process to predict the static properties of telechelic supramolecular systems based on linear precursors.[24] However, the considered one-dimensional diffusion process is far different from the quantitative relaxation mechanisms that are nowadays established for linear chains.[26] Recently, van Ruymbeke et al. have decomposed the effect of supramolecular bonds from the dynamics of entangled polymer precursors and specifically their temperature dependence by including the dynamic association/dissociation or "blinking" of supramolecular associative units in the traditional tube-based model.[27] The relaxation of the polymer precursor is considered to be significantly faster than the reassociation of the associative groups, which means that the polymer segments relax as soon as the supramolecular bonds open. This way, the dynamic change in the structure of the relaxing units can be neglected. In most of the other modeling efforts on main-chain telechelic supramolecular polymers, by contrast, the dynamic blinking itself is neglected and its effect on the topology of the system is replaced by an equivalent average number of permanent bonds.[28−30]

For the other class of side-chain supramolecular polymer network systems, modeling approaches have been more successful. Despite a mismatch in the plateau region, the sticky Rouse model has been frequently reported to provide a good prediction of the linear rheological properties for systems based on unentangled precursors.[12,31−33] For entangled systems, however, the sticky reptation and other models such as sliplink or time marching algorithm (TMA) have had a lower record of successful application, and the need for the synthesis of well-defined supramolecular side-chain associating polymer network systems is more sensible.[8,25,34,35] Normally, the different temperature dependencies of the supramolecular motifs and the dynamics of the polymer precursors prohibit construction of a unique rheological master curve, and even in a homogeneous system, the slow dynamics of the entangled associative chains significantly prolongs the establishment of a thermodynamically equilibrated state.[8,36,37] Accordingly, Shivokhin et al. have delicately utilized a supramolecular system in concentrated solutions, where the effect of both entanglement and supramolecular dynamics could be investigated.[10] However, in most of the studies in the melt, specifically those on systems with strong supramolecular motifs, the formation of ill-defined clusters with significantly longer relaxation times, which dictates the rheological behavior, is inevitable.[11,37,38] Recently, Hawke et al. have shown that the impact of such collective assemblies could be understood and modeled in the framework of tube-based models.[36] Nevertheless, decoupling of the effects of collective assemblies from binary associations is still an open challenge that requires the development of a well-defined supramolecular polymer network model system as a basis for studies.

Motivated by these open questions and based on our former experience on supramolecular polymer network systems with strong side-chain 2-ureido-4[1H]-pyrimidone (UPy) motifs, we have devised a model system where the excessive formation of clusters is hindered. This system is based on poly(lauryl methacrylate) in which a long 12-carbon dangling group shields and suppresses the extensive aggregation tendency of UPy motifs, in contrary to the shorter n-butyl methacrylate or acrylate monomers, where the whole relaxation spectrum is affected by the presence of large UPy clusters.[31,32,37] Then, based on the experimentally observed rheological properties of this system, we introduce a tube-based model to explain the relaxation mechanisms and to decouple the effects of binary associations from those of collective assemblies of UPy stickers. The paper is structured as follows. After a brief description of the synthesis procedure and the devised samples in Section II, we review the important rheological features of the samples and accordingly devise our modeling approach in Section III. In Section V, we confront the model predictions with the experimental data and deconvolute the contribution of binary associations from collective assemblies.

II. EXPERIMENTAL SECTION

Details of the polymerization and postpolymerization grafting of copolymers with UPy motifs can be found in another comprehensive report.[39] In brief, random copolymers of lauryl methacrylate (LMA) and 2-(trimethylsilyloxyl)ethyl methacrylate (TMS-EMA) are synthesized by atom transfer radical polymerization (ATRP) using ethyl-α-bromoisobutyrate (EBriB), *N*,*N*′,*N*″,*N*″-pentamethyldiethylenetriamine (PMDETA), and copper(I) bromide (CuBr) as initiator, ligand, and catalyst, respectively, with a feed composition of 90 mol % LMA. The relative number-average molar mass, M_n, and the polydispersity indexes (PDI) are determined by size exclusion chromatography (SEC), and the chemical compositions of the resultant copolymers are determined based on ^{1}H NMR spectroscopy in $CDCl_3$: LMA in P(LMA-*ran*-TMS-EMA): δ = 3.94 (s, 2H, $COOCH_2CH_2$), 2.10−1.72 (m, 2H, CH_2CCH_3), 1.63 (s, 3H, CH_2CCH_3), 1.31 (d, J = 14.3 Hz, 20H, $COOCH_2CH_2$), 0.90 (t, J = 6.7 Hz, 3H, $CH_2CH_2CH_3$) ppm and TMS-EMA in P(LMA-*ran*-TMS-EMA): δ = 4.13 (s, 2H, $COOCH_2CH_2$), 3.85 (s, 2H, $COOCH_2CH_2$), 2.10−1.72 (m, 2H, CH_2CCH_3), 1.63 (s, 3H, CH_2CCH_3) ppm.

Supramolecular networks are prepared by postpolymerization functionalization of the copolymers made in the previous step with UPy-hexylisocyanate groups in two steps.[39] First, the protecting TMS caps are cleaved at acidic conditions, and then, the UPy motifs are grafted through a urethane linkage. The extent of UPy functionalization is controlled by the fraction of the UPy groups in the feed. The final fraction of grafted UPy motifs in the copolymers is determined by ^{1}H NMR spectroscopy in $CDCl_3$: UPy-grafted units: δ = 13.17 (s, 1H, CHCNH), 11.91 (s, 1H, $CH_2NHCONH$), 10.20 (s, 1H, $CH_2NHCONH$), 5.86 (s, 1H, CHCNH), 3.26 (s, 2H, $CH_2NHCONH$)), 3.11 (s, 2H, CH_2NHCOO) ppm.

Three precursors with different molar masses are synthesized and further grafted with three different percentages of UPy motifs, systematically increasing from 3 to 10 mol %. The samples are coded as P*x*U*y* where the *x* and *y* denote the average number of entanglements and the molar fraction of UPy moieties, respectively. Details of the structural properties of each sample are listed in Table 1. The average mole fraction and the average number of UPy groups per chain are designated by f_{UPy} and N_{UPy}, respectively. The inverse application of the classical time marching algorithm (TMA) suggests a value of 15.3 kg mol^{-1} as the entanglement molar mass of the precursors.[39] Therefore, these precursors cover a range of samples from weakly entangled to well-entangled systems.

Thermal properties of the networks are studied by differential scanning calorimetry (DSC) at a heating and cooling rate of 10 °C min^{-1}. For each measurement, the sample is first heated to 100 °C to

DOI: 10.1021/acs.macromol.9b00323
Macromolecules 2019, 52, 5255−5267

Table 1. Microstructural Parameters, Flow Properties, and Glass Transition Temperatures of the Supramolecular Polymer Networks and the Corresponding Precursor Copolymers Investigated in this Work[a]

sample	M_n (kg mol^{-1})	PDI	f_{UPy} (mol %)	N_{UPy}	E_a (kJ mol^{-1})	$E_{a,LF}$ (kJ mol^{-1})	$E_{a,HF}$ (kJ mol^{-1})	T_g (°C)
P2U0	42.5	1.31	0	0	110			−61.5
P2U3			3.15	5.5	111	111	124	−60.4
P2U5			4.95	8.7	117	114	128	−60.5
P2U10			8.91	15.6	124	113	137	−56.1
P5U0	76.4	1.56	0	0	112			−62.0
P5U3			2.79	8.8	118	118	125	−57.3
P5U5			4.41	13.9	122	112	141	−56.0
P5U10			10.20	32.2	124	117	138	−56.2
P11U0	165.4	1.90	0	0	118			−59.2
P11U3			3.61	24.7	111	111	130	−60.4
P11U5			5.24	35.8	116	110	124	−58.2
P11U10			10.02	68.5	112	110	122	−58.0

[a]Flow activation energies are obtained by time−temperature superposition of all rheological measurements (E_a) or separate overlay of only the data collected below ($E_{a,LF}$) and above ($E_{a,HF}$) the partner exchange time.

erase any thermal history and to provide a reference condition, cooled to −90 °C, and heated again to 100 °C. No first-order thermal transition was witnessed for any of the samples. The glass transition temperatures are determined from the result of the second heating ramp, as listed in Table 1. ATR FTIR spectroscopy is performed on a Jasco FT/IR-4000 using 32 scans.

I) Linear viscoelastic responses of the precursor copolymers and the supramolecular networks are measured using a stress-controlled Anton Paar MCR 302 rheometer equipped with parallel plate geometry (gap size, 100−400 μm; plate diameter, 8 mm). Before each measurement, the sample is monitored for 30 min (γ = 1%, ω = 1 rad s^{-1}) to make sure that the sample is at equilibrium. Subsequently, the linear viscoelastic regime is determined by an amplitude-sweep at a constant frequency (γ = 0.1−20%, ω = 1 rad s^{-1}). After another time sweep experiment (30 min, γ = 1%, ω = 1 rad s^{-1}) to monitor the sample re-equilibration, frequency sweep measurements are performed at multiple temperatures between 5 and 105 °C at a constant strain amplitude (γ = 1%, ω = 0.01−100 rad s^{-1}). The iso-friction master curves at a reference temperature of 25 °C are constructed in two steps. First, the dynamic moduli obtained at different temperatures are horizontally shifted to match the measurement at the reference temperature. Then, the master curves of all supramolecular polymer networks are horizontally shifted to overlay with their corresponding precursor polymer in the high-frequency region. The flow activation energies (E_a) are determined based on an Arrhenius relationship, and results are listed in Table 1.

III. MODELING

III.A. Classical Time Marching Algorithm. The time marching algorithm (TMA) is a tube-based model that can successfully predict the rheological properties of nonassociative linear and branched polymer structures.[14−16] The main difference between TMA and other tube-based models is that it includes all relaxation mechanisms in parallel, without any need for time−space separation of different mechanisms.[40] In our earlier work,[39] we inversely used this model to determine key material parameters of the synthesized copolymers, that is, the entanglement molar mass, M_e, plateau modulus, G_N^0, and Rouse relaxation time of an entanglement strand, τ_e, by minimizing the difference between model predictions and the experimentally measured dynamic moduli of the unfunctionalized precursors. Details of such a model implementation are described elsewhere.[22,39] The obtained optimal values for M_e, G_N^0, and $\tau_e$were 15.3 kg mol^{-1}, 0.114 MPa, and 85 ms, respectively.

III.B. Experimental Observations. The dynamic moduli of the synthesized supramolecular polymer networks are shown separately for different molar masses in Figure 1. At first glance, the overall behavior follows the trend that is expected from a side-chain supramolecular polymer network according to the established tube-based models.[8,12,25] However, several deviations become apparent upon a detailed investigation of the relaxation steps. Before rushing into the modeling approach and describing the model development steps, we review some of the most important, rather unexpected, observations.

(a) In some of the supramolecular polymer systems reported in the literature, the first relaxation process, after the high-frequency Rouse relaxation, is attributed to the relaxation of unfunctionalized chains.[27,36] Such relaxation occurs at the frequency where the precursor chains disentangle.[29,30] This relaxation can be differentiated from the general two-step relaxation behavior of the sticky reptation mechanism[12,41] as the subsequent plateau modulus is not associated with the entanglement plateau but depends on the fraction of functionalized chains, instead. By precise inspection of the iso-friction master curves of the samples, functionalized with different extents of supramolecular associative UPy motifs, it can be confirmed that there is no sign of relaxation at the specific relaxation frequency of the precursors. The red dashed lines in Figure 1 denote the terminal relaxation time of the precursors, based on the observed $G'-G''$ crossover, and we see that at these points, no peak or shoulder is apparent in the loss moduli of the corresponding supramolecular systems, except for the P11 series in which this coincides with the onset of relaxation. We conclude from these findings that all chains are similarly functionalized.

(b) The blue dashed lines, going through all peaks in the loss moduli of the supramolecular polymer networks, show that the onset of relaxation happens almost at the same time for all supramolecular systems, independent of their UPy content. This relaxation time is longer than the relaxation time of the weakly entangled precursor, P2U0, while it is shorter than the relaxation time of the well-entangled P11U0. Just like all side-chain supramolecular systems, such relaxation can be attributed to the dissociation of the UPy hydrogen bonding or more precisely to their effective partner exchange time, τ_{ex}, since going back to the former partner does not contribute to stress relaxation.[25,27,34] A similar behavior has been

DOI: 10.1021/acs.macromol.9b00323
Macromolecules 2019, 52, 5255−5267

frequently described in the context of the sticky Rouse mechanism.[32,42,43]

(c) The high-frequency plateau increases with the UPy content but reaches a steady level sooner for longer precursors. The high-frequency plateau is frequently correlated to the total amount of network junctions formed by both supramolecular associations and entanglements.[8,10,25,36] From its high level, we can conclude that the density of stickers is larger than the density of entanglements. The second plateau is beyond the accessible frequency range for the samples P5U5, P11U3, and P11U5, but it can be inferred from the slopes of the dynamic moduli at low frequencies. A similar behavior was already observed for samples made from various UPy motifs.[39] This second plateau is well below the entanglement plateau of the precursors and is typically attributed to the fraction of entangled segments that are trapped between long-lasting large collective assemblies of supramolecular associations.[33,36,38]

(d) In cases where collective assemblies form a perceptible low-frequency plateau, the dynamic moduli drop in parallel from the high- to the low-frequency plateau with a log−log slope close to 0.5, as expected from a Rouse relaxation mechanism. We have already explained this regime by contour length fluctuations (CLF) of side-chain supramolecular polymers including the dynamic association/dissociation of supramolecular bonds.[8] This leads to a slow Rouse-like relaxation from the high- to the low-frequency plateau.

Based on these observations, we can highlight the main differences between the detected and expected rheological behaviors. Normally, the drop in the storage modulus, as a result of dissociation of binary supramolecular associations, continues until the emergence of the entanglement plateau, followed by a molar-mass-dependent relaxation process,[9,44] according to the sticky reptation mechanism[25,34] as schematically depicted by red lines in Figure 2. This process leads to the final relaxation, in the absence of collective assemblies (dotted line), or continues to the low-frequency plateau that correlates with the fraction of entangled segments that are trapped between long-lasting aggregates. Surprisingly, in the current series of samples (represented by green lines in Figure 2), all chains start to relax almost independently of their molar mass, and the high-frequency plateau is directly followed by the terminal relaxation (dotted line) or by the low-frequency plateau, without any indication of the entanglement plateau. That means that, in contrast to the sticky reptation model, all mobile sticky segments disentangle before or in parallel to the partner exchange process. As discussed in Section V, a possible explanation for this behavior could be a very long effective partner exchange time of the stickers, compared to their real lifetime, that is, a system is much more mobile than it is effectively seen in the rheological curves.[45]

These observations suggest that the classical modeling approaches that have been established for describing the rheological behavior of side-chain supramolecular polymer network systems cannot explain all the detected rheological aspects.[8,10,25] In particular, the effective partner exchange time cannot be used to determine the disentanglement time of the chains. Therefore, in this paper, we rather consider that the stickers, which are present in large amount all along the polymer, lead to an overall delay in the relaxation processes of the chains due to the enhanced friction they generate. This delay is unknown and is determined by the best fitting procedure. The components of this model are first outlined in the Section III.C and the details are then presented in Section III.D.

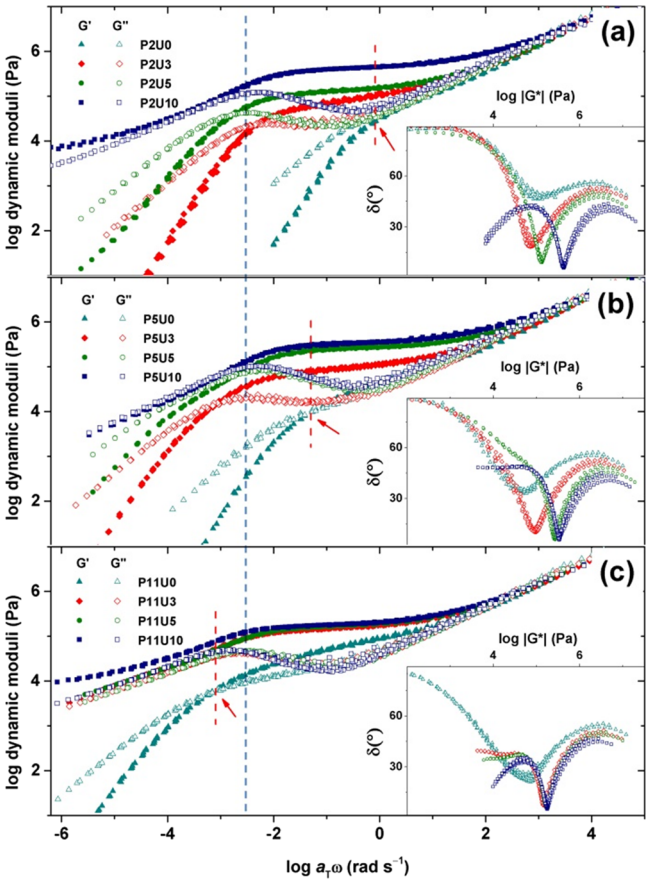

Figure 1. Comparison of the iso-friction master curves of the dynamic moduli of the precursors with the corresponding supramolecular polymer network systems for (a) P2, (b) P5, and (c) P11 sample series. Red arrows and red dashed lines denote the terminal relaxation time of each precursor, and the blue dashed line indicates the approximately parallel onset of relaxation in the supramolecular polymer networks based on the observed peaks in the loss moduli. Inset plots show the van Gurp−Palmen curves of the same sample series.

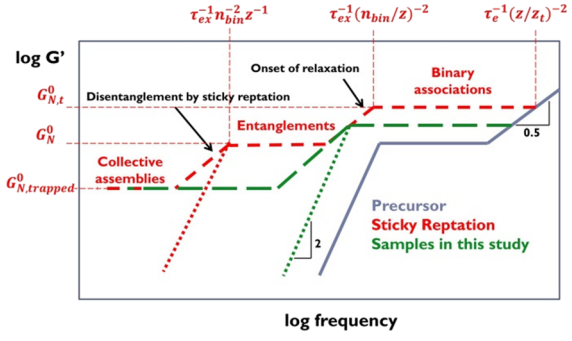

Figure 2. Schematic representation of different relaxation steps as reflected in the storage modulus of the precursor (blue), the established model, including sticky Rouse and sticky reptation mechanisms (red), and the experimental behavior of the samples in this study (green). The dotted lines denote the terminal relaxation in the absence of collective assemblies.

DOI: 10.1021/acs.macromol.9b00323
Macromolecules 2019, 52, 5255−5267

III.C. Modeling Outline. According to the described observations, from high to low frequencies, the following relaxation mechanisms should be considered:

Fast Rouse relaxation can proceed at high frequencies up to the length of strands located between binary associations and entanglements, which relaxes at a timescale of $\tau_e(z/z_t)^2$, where z and z_t denote the number of entanglements and the number of entanglements plus binary associations, respectively.

Depending on temperature, only a fraction of stickers is active at a time. This fraction is determined by the association equilibrium constant and the topological constraints imposed by entanglements. For this reason, the high-frequency plateau modulus does not increase as much as expected from the total number of grafted supramolecular associative groups. We therefore determine the average density of associated stickers, f_{bin}, from the level of this high-frequency plateau. Segments that are placed between the free chain ends and the outermost active stickers, hereafter called dangling ends, have the possibility to relax by CLF with no extra delay due to the stickers. Even for chains with a large number of stickers, there is a notable fraction of free stickers, and accordingly, of free dangling ends, as highlighted in blue in Figure 3. These segments relax right after the high-frequency Rouse modes and do not contribute to the high-frequency plateau.

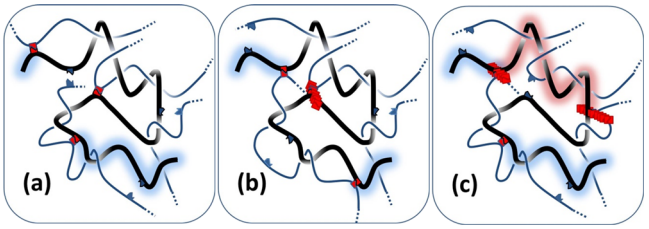

Figure 3. Classification of chains based on the number of collective assemblies: (a) free chains without collective assembly, (b) star-like chains with one collective assembly, and (c) chains having more than one collective assembly, which consist of mobile and frozen (highlighted in red) segments. Dangling ends between the outermost active stickers and the chain extremities, highlighted in blue, are free to relax at high frequencies. The rest of the segments can relax (with higher friction) only after dissociation of binary stickers, except for the frozen segments that are trapped between collective assemblies.

In the absence of collective assemblies, all chains become mobile and start to disentangle right after dissociation of binary stickers. For weakly entangled chains, this relaxation happens according to the second step of the sticky Rouse mechanism. Well-entangled chains disentangle by reptation and CLF but with higher friction due to the dynamic blinking of binary stickers. As already mentioned, this is taken into account by a global slowing down of the CLF mechanism. Following our former approach for modeling the relaxation of side-chain supramolecular polymer networks, we neglect the sticky reptation for linear chains and instead consider delayed fluctuations as the main relaxation mechanism.[8]

In the presence of collective assemblies, chains are divided into three groups: those with zero, one, or more than one collective assembly, as schematically shown in Figure 3. Chains with zero and chains with one collective assembly (Figure 3a,b) relax like linear and star-like chains, respectively, while chains with more than one collective assembly (Figure 3c) consist of mobile and frozen segments. The segments placed between the chain extremities and the outermost collective assemblies are named sticky dangling ends. They relax by CLF, like the arms of a star-like chain. Frozen segments, trapped between outermost collective assemblies (highlighted in red), however, are incapable of relaxation. Correspondingly, the relaxation of all mobile segments is slowed down by the extra friction coming from the blinking stickers, whereas it is accelerated by the fraction of dangling ends that are relaxed at higher frequencies.

We assume that the stress corresponding to the weight fraction of the segments trapped between two collective assemblies does not relax at the experimentally measured frequency range, even after application of time−temperature superposition (tTs). The fraction of trapped segments determines the height of the low-frequency plateau. Following our earlier approach,[36] we determine the density of collective assemblies based on the fraction of trapped segments, which is itself determined based on the level of the low-frequency plateau.

III.D. Model Description. As outlined in Section III.C, the essential relaxation mechanisms that are required for interpreting the experimental behavior of the supramolecular polymer networks in the presence of collective assemblies include (I) sticky Rouse relaxation, (II) CLF of dangling ends at high frequencies, and (III) relaxation of mobile segments, that is, the molecular segments that are not trapped between two collective assemblies and that can relax with a global delay at the rhythm of the association/dissociation of binary stickers. After describing the details of each mechanism in Section III.D.1, we describe the statistical model that relates the fraction of trapped segments to the probability of a sticker to be a part of a collective assembly in Section III.D.2.

III.D.1. Details of Essential Mechanisms. The classical Rouse model for the relaxation of entangled polymer chains is divided into two types of modes: three-dimensional modes for the length scales below the entanglement spacing and one-dimensional longitudinal modes beyond that scale.[26] In the presence of supramolecular associations, however, the three-dimensional fast modes can only proceed up to the length scale between two adjacent network junctions, formed either by entanglements and binary stickers. At these length scales, the presence of stickers is not yet essentially felt, and the relaxation proceeds in a conventional fashion, that is, according to the monomeric friction. Nevertheless, the longer Rouse modes are delayed by the lifetime of the binary associations and are slowed down due to the extra friction coming from the blinking stickers. We neglect these longitudinal long-range Rouse modes in the presence of stickers as it involves coordinated motion of several sticky groups, which takes a significant time to achieve.[8]

$$\varphi_{\text{Rouse,fast}}(t) = \sum_{p=z_t+1}^{N} \exp\left(\frac{-2p^2 t}{\tau_{\text{R,fast}}}\right) \quad (1)$$

$$\varphi_{\text{Rouse,sticky}}(t) = \sum_{p=z}^{z_t} \exp\left(\frac{-p^2 t}{\tau_{\text{R,sticky}}}\right) \quad (2)$$

Equation 1 scans the length scales from a monomer to a network strand between entanglements and binary stickers,

DOI: 10.1021/acs.macromol.9b00323
Macromolecules 2019, 52, 5255−5267

according to the monomeric friction. Equation 2 adds the modes up to the entanglement length at the rhythm of the stickers' blinking. The utilized timescales are defined as

$$\tau_{R,fast} = \tau_e z^2 \tag{3}$$

$$\tau_{R,sticky} = \tau_{es} z^2 \tag{4}$$

$$\tau_{es} = \max\left(\tau_e, \tau_{ex}\left(\frac{M_e}{M_{bin}}\right)^2\right) \tag{5}$$

where τ_{ex} is the effective partner exchange time for binary stickers, and $M_{bin} = \frac{M_w}{(N_{bin}+1)}$ is the weight average molar mass of the strand between two adjacent stickers, while $N_{bin} = f_{bin}N$ is the number of active binary stickers per chain, whereby N stands for the degree of polymerization, and f_{bin} is the mole fraction of active binary sticker associations. The number of active binary stickers is always lower than the number of incorporated UPy motifs ($f_{bin} < f_{UPy}$) since not all the grafted units actively contribute to the formation of supramolecular bonds. This means that at each specific time, only a few stickers are attached, and the other "nonactive stickers" are unattached and available to create new associations through partner exchange. However, it is likely that a sticker that is trapped in an association has to associate and dissociate several times to its old partner before becoming able to hop to another place.[46] Therefore, the effective exchange time is usually longer than what could be obtained from the measured association energy. However, in the model, there is no need for the dissociated stickers to come back to the old partner. Consequently, we only consider the effective partner exchange process.

The total number of network junctions formed by both entanglements and binary associations is defined as $z_t = \frac{M}{M_{et}}$, similar to the definition of the number of entanglements, $z = \frac{M}{M_e}$. The effective network strand length between junctions formed by both entanglements and binary associations is defined as

$$M_{et}^{-1} = M_e^{-1} + M_{bin}^{-1} \tag{6}$$

Relaxation of dangling ends starts right after the fast Rouse modes. They relax simply by CLF; however, they are slowed down because all segments placed between the outermost active stickers are frozen and do not participate in dynamic dilution, that is, the unrelaxed fraction of chains is defined as $\Phi(s) = \nu_{end}(1 - s) + (1 - \nu_{end})$, which is used for calculating the potential penalty of retractions

$$U(x) = 3k_B T z_{end} \int_0^x s\Phi^{\alpha}(s)\mathrm{d}s \tag{7}$$

where ν_{end} and z_{end} denote the weight fraction and number of entanglements of the dangling ends. In addition, α, the dilution exponent, has a value between 1 and 4/3[47] and is considered to be 1 in this work.[14,15,47] Here, x is the dimensionless position of each segment, which changes from zero at the free end to one at the middle of the chain for linear chains or to one at the frozen branching point or the supramolecular linkage, in the case of star chains or dangling ends. The specific CLF lifetime is determined by free Rouse motions of the segments near the chain extremities, while deeper segments need to overcome the potential penalty of retractions. The transition between two modes happens at the segment where the penalty is equal to the environmental thermal energy. The lifetimes of these two CLF modes are defined as

$$\tau_{early} = \frac{9\pi^3}{16}\tau_e z_{end}^4 x^4 \tag{8}$$

$$\tau_{late} = \tau_0 \exp\left(\frac{U(x)}{kT}\right) \tag{9}$$

Therefore, the fluctuations time, $\tau_{fluc}(x)$ takes the value of τ_{early} or τ_{late} depending on the position of the segment. According to the original TMA model, τ_0 is defined so that there is no discontinuity in the CLF characteristic time, switching from the early to the late modes.[16] The CLF process of dangling ends is described by the following probability

$$p_{fluc,end}(x, t) = \exp\left(\frac{-t}{\tau_{fluc,end}(x)}\right) \tag{10}$$

The CLF relaxations of all the molecular segments, which require the association/dissociation of the stickers to disentangle, are slowed down by the global retraction penalty, p_{free}, due to the blinking effect of the supramolecular bonds. Only the chain segments that are not trapped between two assemblies can relax via this process. The CLF process of these segments is explained by the following probability

$$p_{fluc,i}(x, t) = \exp\left(\frac{-p_{free}t}{\tau_{fluc,i}(x)}\right) \tag{11}$$

and the overall chain survival probability is defined as

$$\varphi_{chain}(t) = \nu_t + \sum_i \nu_i \int_0^1 p_{fluc,i}(x, t)\mathrm{d}x,$$
$$i = \text{end, linear, star, dangling} \tag{12}$$

where the summation is performed on dangling ends (coded as end) relaxing at high frequencies and emerging free chains including linear, star, and sticky dangling ends (coded as dangling). In the absence of collective assemblies, the summation is performed only over dangling ends and linear chains.

After the second step of the sticky Rouse mechanism and chain disentanglement, the dynamic moduli may directly enter the terminal zone in the absence of collective assemblies or drop from the high-frequency plateau to the low-frequency plateau, in their presence. The high-frequency plateau, $G_{N,t}^0$, correlates with the network strand length (assessed by its molar mass M_{et}), while the low-frequency plateau, $G_{N,trapped}^0$, scales with the weight fraction of the trapped segments (ν_t)

$$\frac{G_{N,t}^0}{G_N^0} = \frac{M_e}{M_{et}} \tag{13}$$

$$G_{N,trapped}^0 = G_N^0 \nu_t^{1+\alpha} \tag{14}$$

As the global effect of constraint release, the tube itself can relax by lateral Rouse-like motions, according to its survival probability. The tube relaxation happens at the same rate as the overall chain relaxation but not faster than what the Rouse process allows[16]

DOI: 10.1021/acs.macromol.9b00323
Macromolecules 2019, 52, 5255−5267

$$\varphi_{\text{tube}}(t_i) \geq \varphi_{\text{chain}}(t_{i-1})\left(\frac{t_{i-1}}{t_i}\right)^{0.5} \quad (15)$$

Eventually, the relaxation modulus reads as

$$\frac{G(t)}{G_N^0} = \frac{1}{z}(\varphi_{\text{Rouse,fast}}(t) + \varphi_{\text{Rouse,sticky}}(t)) + \varphi_{\text{chain}}(t)\varphi_{\text{tube}}(t)^{\alpha} \quad (16)$$

Similar to our former works,[14−16] we use Schwarzl's approximation to convert the transient modulus to dynamic moduli.

III.D.2. Statistical Model. Finally, a statistical model is developed to correlate the weight fraction of trapped segments, ν_t, to the number of collective assemblies. For this purpose, we randomly draw chains out of a log-normal distribution of chain lengths, and each monomer of each chain is checked for the probability of forming a collective assembly. In more detail, a random number is generated, and if its value is below the considered threshold, that is, f_{col}, the monomer is considered as a long-lasting junction. The segments that are located between two outermost collective assemblies are classified as trapped, while the ones that are located beyond the outermost collective assemblies, on each side of the chains, are named sticky dangling ends or mobile molecular segments. In addition, chains containing zero or just one collective assembly are separately classified as linear and star-like chains, respectively. The best f_{col} values are obtained by optimization so that the ν_t values from the tube-based model and the statistical model match. The probability for a monomer to be part of a collective assembly is affected by the presence of entanglements, as demonstrated in the next section; however, the correlation between ν_t and f_{col}, is independent of the relaxation dynamics.

The evolution of the weight fraction and weight average degree of polymerization (DP_w) of different classes of segments as a function of f_{col} for a polymer with number average degree of polymerization (DP_n) of 500 and PDI of 1.5 is shown in Figure 4. This representative sample is in the range of the average length and dispersity of the samples studied here. The fraction of linear chains decreases opposed to the fraction of trapped segments, while the fractions of star and sticky dangling end segments go through a maximum and diminish as f_{col} increases from 0 to 1, as shown in Figure 4a. At the same time, the length of mobile segments decreases, while the length of trapped segments grows to a constant value, as displayed in Figure 4b. Notably, this constant value is larger than the average length of the precursor as longer chains make larger contributions to the formation of trapped segments, while shorter chains have a higher chance to become a star-like or a linear chain. This effect is amplified at higher PDI values. As an example, Figure 4c,d shows the obtained weight distributions of molar mass for different classes of segments for two f_{col} values of 0.01 and 0.001. Logically, while the weight distribution of the star-like chains remains at the same abscissa and only change in height, the distribution of sticky dangling ends and trapped segments move in opposite directions by changing the value of f_{col}.

IV. RESULTS AND DISCUSSION

The material basis for our studies is a set of copolymers composed of LMA and HEMA, which are randomly grafted with strongly associating UPy units. We systematically vary the chain length and the fraction of supramolecular groups to investigate

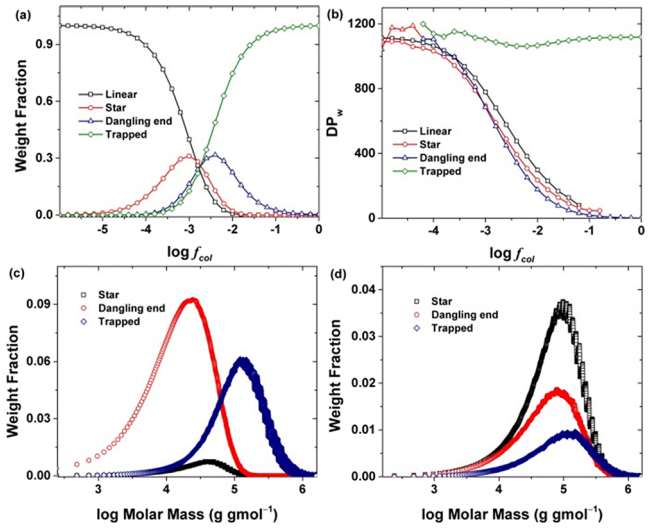

Figure 4. Evolution of (a) the weight fraction and (b) the weight average degree of polymerization of different classes of segments as a function of f_{col} and evolution of the weight distribution of molar mass for different classes of segments: star-like arms, sticky dangling ends, and trapped segments for (c) f_{col} = 0.01 and (d) f_{col} = 0.001, for a precursor defined by DP_n = 500 and PDI = 1.5.

the simultaneous effects of the supramolecular associations and the polymeric dynamics on the rheological properties. The details of the synthesis approach and the corresponding assignment of ^{1}H NMR peaks, which can be used for quantitative determination of the UPy content of the copolymers, are illustrated in Figure 5. In a traditional acrylate or methacrylate system, such a high fraction of strong UPy motifs leads to strong aggregations that dominate the rheological behavior in the entire frequency range.[7,37,48] In this work, a long 12-carbon pendant group on the LMA monomer serves to shield the UPy motifs and diminish large-order orientations. Such a long pendant group has about a quarter of the length of an entanglement strand; therefore, a binary association is half as long as an entanglement strand. Hence, there is some freedom of movement of the chain at the point of attachment. This means that the sticky groups are not point-like, and therefore, the real number of active binary stickers is slightly higher than what can be obtained from eq 13. However, quantifying this effect is beyond the capability of tube-based models and needs more in-depth molecular dynamics simulations.

The large-order orientation of UPy groups is expected to show distinct melting points, depending on the size of the formed stacks.[37,49,50] To characterize the melting properties of our supramolecular polymer system, we record DSC thermograms. The obtained thermograms do not show any first-order melting transition, which implies the absence of significantly large UPy clusters.[37] We denote that the collective assemblies of the associative groups, which are accredited for the appearance of the low-frequency plateau modulus in the rheological spectrum, are also kind of UPy clusters. These clusters have significantly longer lifetimes compared to the simple binary association; however, they are not large and abundant enough to make distinct melting points. The glass transition temperatures of the supramolecular copolymers are also calculated from the DSC thermograms, as listed in the last column of Table 1. The unfunctionalized copolymer is an amorphous rubber, which is flexible at room temperature due to its low glass transition temperature (T_g = −61 °C). The supramolecular copolymers

DOI: 10.1021/acs.macromol.9b00323
Macromolecules 2019, 52, 5255−5267

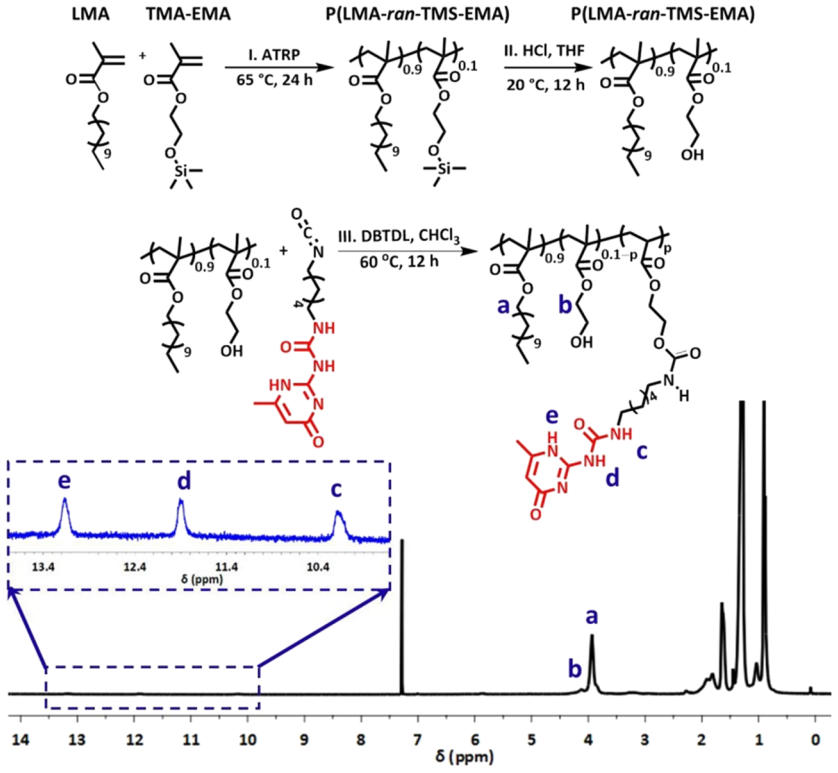

Figure 5. Synthesis of the supramolecular polymer network systems studied in this work: three-step approach including (i) ATRP copolymerization of LMA and TMS-EMA followed by (ii) hydrolysis of the protecting TMS cap and (iii) grafting of the UPy moieties; typical ^{1}H NMR spectrum of a supramolecular polymer network, where the characteristic peaks of the grafted UPy groups are further highlighted.

also show a similar behavior. However, the measured T_g values slightly increase for copolymers with higher UPy fraction, confirming the hindrance of chain mobility in the presence of bulky UPy groups.[32,33,37]

To provide further confirmation for the presence of such ordered assemblies, we record the FTIR absorption spectra and follow their trends. The stretching vibrations of the carbonyl groups, which belong to the LMA and EMA repeating units, as well as the UPy motifs, can be observed in a range between 1600 and 1800 cm^{-1}. The signals around 1730, 1700, and 1660 cm^{-1} can be respectively assigned to the non-hydrogen-bonded, disorderly bound, and the orderly bound carbonyl groups, as shown in Figure 6 for the P5 samples series and in Figure S1 for the P2 and P11 sample series. Specifically, the intensities of the hydrogen-bonded carbonyl groups, at 1700 and 1660 cm^{-1}, increase monotonically with the UPy fraction.

To investigate the interplay of the dynamics of entangled polymer chains and transient association in the presence of collective assemblies, we use dynamic rheological measurements. The different temperature dependencies of the polymeric and the supramolecular dynamics typically results in thermorheological complexity. This usually limits the application of the time−temperature superposition principle for the entangled supramolecular polymeric systems.[36,37] The van Gurp−Palmen plot of the damping factor against the complex modulus is a sensitive measure of thermorheological complexity.[51] The graphs obtained for our supramolecular polymer samples are shown in the inset plots of Figure 1. It is clear that none of the samples possess notable thermorheological complexity at the low modulus region, which corresponds to low frequencies. Therefore, we use the least-squares method to horizontally shift the measurements obtained at different temperatures and to

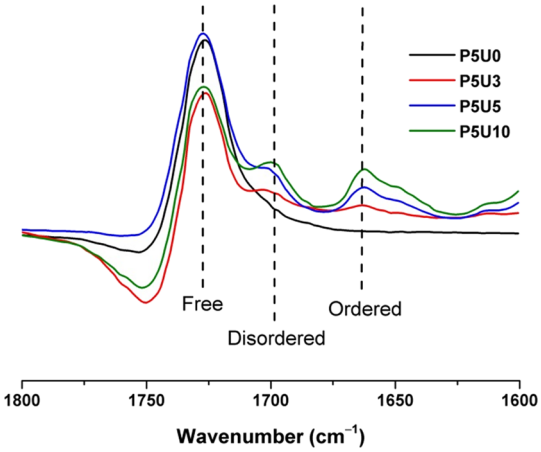

Figure 6. FTIR spectra of the P5 sample series in the range of the carbonyl bond stretch vibrations. Non-hydrogen-bonded, disorderly bound, and orderly bound groups can be discriminated based on their distinct adsorptions.

construct master curves of the dynamic moduli at a reference temperature of 25 °C. All master curves of the supramolecular polymer networks are then horizontally shifted to overlap with their corresponding precursor polymer data at high frequencies to obtain the so-called iso-friction master curves. Nonetheless, thermorheological complexity is slightly perceptible at higher frequencies, where the dangling ends are expected to relax. This is not surprising since the number of active stickers and, accordingly, the length of the dangling ends vary with the temperature. To put it simply, a higher temperature decreases the association tendency, and a larger fraction of segments becomes mobile as dangling ends.

DOI: 10.1021/acs.macromol.9b00323
Macromolecules 2019, 52, 5255−5267

The obtained iso-friction master curves of the supramolecular polymer network systems are compared to their parent precursors, separately for different molar masses, in the main plots of Figure 1. The precursors show a broad relaxation spectrum as expected from their relatively high PDI values. In contrast, the supramolecular polymer networks show a flat plateau and distinct relaxation steps, as discussed in Section III.C. This relaxation is mainly governed by the binary associations, which are homogeneously distributed along the chains. Consequently, the PDI value has a smaller influence on the rheological properties of the supramolecular polymer networks. While the terminal relaxation times of the precursors differ by more than 3 orders of magnitude, all supramolecular polymer networks start their relaxation almost at the same time, independently of their UPy content. As a result, this relaxation step is recognized as the partner exchange time of the active binary UPy associations. All segments, except those trapped between collective assemblies, are expected to show a relaxation that is slowed down due to the extra friction coming from sticky side groups. As already explained, the absence of such a molar-mass-dependent relaxation step suggests that their disentanglement is faster than what a classical sticky reptation model predicts. We explain this slow relaxation by a CLF process, which is delayed by a global retraction penalty. This is like if the whole chain feels more friction due the repetitive association and dissociation of its stickers that are placed all along the backbone. To properly describe the CLF of these sticky chains, we have to rescale the τ_e parameter in a way that the disentanglement process takes place nearly at the same time as the sticky Rouse modes do. Due to this simultaneity of both relaxation processes, no entanglement plateau is discernible. This explanation is justified as the chains are only poorly entangled. In addition, as the samples are polydisperse, the relaxation of short chains accelerates the disentanglement of long ones by providing extra solvent in the system. Still, the lack of an entanglement plateau is indeed difficult to understand, and a more conclusive discussion could be made by studying monodisperse longer chains.

From the rheological curves, four unknown parameters can be determined to characterize the samples: (1) the fraction of active binary associations, f_{bin}, is directly determined from the level of the high-frequency plateau modulus, with the help of eqs 6 and 13; (2) their partner exchange time, τ_{ex}, is mainly determined from the onset of supramolecular relaxation; (3) the fraction of trapped segments, ν_t, which is derived from the level of the low-frequency plateau; and (4) the retraction penalty for fluctuation of sticky segments that are not trapped between two collective assemblies, p_{free}. These parameters are optimized in a physically meaningful range to correctly describe the viscoelastic properties of the samples. The obtained fit parameters for all samples are listed in Table 2. The global retraction penalty is inversely proportional to the fraction of active binary stickers, as expected. Besides, the obtained values for τ_{ex} are in the same range in each series and only change between 300 and 1000 s^{-1} in all sample series. Finally, from the value of ν_t, the molar mass and the weight fraction of different classes of sticky chain segments, as well as the probability for a monomer to be part of a collective assembly, f_{col}, can be determined using the statistical model described in Section III.D.2. The obtained results are listed in Table 3.

The absence of thermorheological complexity at low frequencies, especially in the vicinity of the onset of relaxation, supports the idea that the binary stickers dissociate at higher frequencies. This should also increase the flow activation energy.

Table 2. Calculated Fit Parameters, Including the Percent of Binary Associations (f_{bin}), the Partner Exchange Time (τ_{ex}), the Weight Fraction of Trapped Segments (ν_t), and the Global Retraction Penalty (p_{free})[a]

sample	f_{bin} (%)	τ_{ex} (s)	ν_t (%)	P_{free}	f_{col} (%)
P2U3	0.1	745	0.00	0.0509	0.00
P2U5	0.83	714	0.00	0.0002	0.00
P2U10	3.06	633	21.07	0.0001	0.73
P5U3	0.72	450	0.00	0.1678	0.00
P5U5	2.45	303	0.02	0.0081	0.01
P5U10	3.07	313	9.74	0.0032	0.19
P11U3	1.00	990	9.98	0.0700	0.07
P11U5	1.00	969	12.13	0.0680	0.08
P11U10	1.22	999	20.64	0.0418	0.14

[a]The probability of a monomer to be part of a collective assembly (f_{col}) is calculated by the statistical model based on the obtained ν_t.

Accordingly, we try to separately overlay the measurements above and below the onset of relaxation, and the corresponding activation energies are respectively shown by the high-frequency (Ea_{HF}) and the low-frequency (Ea_{LF}) activation energies in Table 1. The low-frequency measurements can be simply overlaid using the same shift factors obtained for the precursors. Nevertheless, the high-frequency measurements need higher activation energies to overlay. This supports our argument that the dissociation of binary stickers at higher frequencies imposes extra activation energy on flow, on top of the one required for the polymeric dynamics. It also demonstrates that there is a difference between the lifetime of binary stickers and the effective partner exchange time as it has been experimentally proven for different supramolecular polymer network systems.[27,43,52,53] In addition, the overall activation energy is known to increase with the UPy content.[37,48] This is indeed observed in our P2 and P5 sample series. However, this trend is not followed in the well-entangled P11 series. This finding suggests that the presence of entanglements limits the density of supramolecular assemblies. We discuss the interplay of entanglements and supramolecular assemblies based on the obtained model parameters in the final discussion.

We have considered the dangling ends, which are located beyond the outermost active stickers, to relax before the modulus enters the high-frequency plateau. As already discussed, the sticky Rouse model has been frequently reported to show a mismatch in the loss modulus in the vicinity of the high-frequency plateau.[12,31,33] This mismatch is attributed to the fact that the system is oversimplified by considering an equidistant placement of binary associations along the backbone. To fix this oversimplification, recently, Cui et al. have developed a stochastic sticky Rouse model that accounts for the intrachain distribution of associative units, which improves the predictions for an unentangled supramolecular polymer system.[31] In addition, Chen et al. have included an interchain comonomer distribution to improve the predictions of sticky reptation for an entangled supramolecular polymer network system.[44] Following these two approaches, we consider the effects of both inter and intramolecular comonomer distributions by random placement of comonomers along chains that are randomly withdrawn from a bivariate distribution of chain lengths and chemical compositions. Details of this approach are described in the Supporting Information. However, for our specific system, the improvement is not significant, as shown in Figure S2. Therefore, the main contributing relaxation

DOI: 10.1021/acs.macromol.9b00323
Macromolecules 2019, 52, 5255−5267

Table 3. Number Average Molar Masses and Weight Fractions of Different Classes of Segments Calculated from ν_t, the Fitted Fraction of Segments Trapped between Two Collective Assemblies

sample	ν_{Linear} (wt %)	ν_{Star} (wt %)	$\nu_{Dangling}$ (wt %)	$\nu_{Trapped}$ (wt %)	M_{Linear} (kg mol^{-1})	M_{arm} (kg mol^{-1})	$M_{Dangling}$ (kg mol^{-1})	$M_{Trapped}$ (kg mol^{-1})
P2U10	25.0	29.7	24.2	21.1	31.6	19.5	14.9	26.0
P5U5	97.3	2.6	0.0	0.0	75.6	59.2	58.3	61.1
P5U10	46.6	30.3	13.3	9.8	59.7	42.1	39.1	57.3
P11U3	48.6	28.5	12.8	10.0	123.0	97.8	104.1	161.9
P11U5	44.1	28.7	14.9	12.2	118.6	93.3	97.2	158.4
P11U10	30.7	27.1	21.3	20.8	104.2	79.1	78.1	152.5

mechanism in this region is accredited to the fluctuations of the dangling ends.

Including the relaxation of dangling ends is crucial for providing a decent description of the dynamic moduli in the high-frequency plateau region. Otherwise, due to the absence of any relaxing structure, the loss modulus could be significantly underestimated in this region, as already reported by the classical sticky Rouse and sticky reptation models.[12,31,44] The average length of the dangling ends is therefore an important parameter that determines the extent of relaxation in the vicinity of the high-frequency plateau. Considering a monodisperse comonomer distribution and an equidistant distribution of active stickers, the exact length of dangling ends would be equal to the distance between active stickers, that is, $M_{end} = M_{bin}$, and their weight fraction can be rationally calculated as $\nu_{end} = \frac{2M_{end}}{M_w}$. The obtained modeling results manifest a significant mismatch in the loss moduli at high frequencies, specifically for the P2U10 and P5U10 samples, as shown in Figure 7. The extra relaxation in these samples could be due to the presence of larger fast-relaxing structures, such as loops, that are not easy to track by characterization methods.

The modeling results obtained by ignoring the presence of collective assemblies are shown by dashed lines. This model can provide a satisfactory match for most of the samples. However, deviations at low-frequency region suggest that the collective assemblies are required for samples with higher UPy contents, even for P11U3 and P11U5 samples that only show power-law decay at low frequencies. The predictions considering the presence of collective assemblies are shown by solid curves. The improvement of predictions at low frequencies is remarkable for the mentioned samples.

The observed experimental behavior and the obtained modeling results reveal the strong difference in the contribution of binary and collective supramolecular associations among different sample series. Consequently, using the obtained model parameters, as listed in Table 2, we elucidate the contribution of binary associations and collective assemblies. Specifically, we calculated the total fraction of active stickers ($\nu_{active} = \frac{f_{col}+f_{bin}}{f_{UPy}} \times 100$) and among them the fraction of collective ones ($\nu_{col} = \frac{f_{col}}{f_{col}+f_{bin}} \times 100$) and determine how these parameters change with the studied microstructural parameters. The obtained values are plotted against the fraction of grafted UPy motifs (f_{UPy}) and the maximum number of network junctions formed by the number of incorporated UPy groups and the entanglements ($N_{max} = N_{UPy} + z$), as shown in Figure 8.

The fraction of active stickers increases at higher UPy contents for the unentangled supramolecular polymer systems, as shown in Figure 8a. This finding shows that the accessibility of

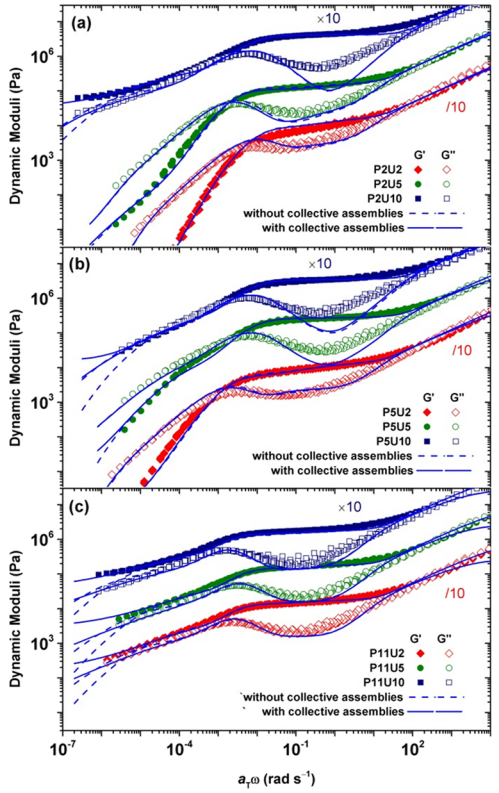

Figure 7. Comparison between experimental data (symbols) and model predictions, including (solid lines) and excluding (dashed lines) the presence of collective assemblies for different samples series: (a) P2, (b) P5, and (c) P11.

the supramolecular associative groups to each other is the first obstacle for the formation of supramolecular bonds, while the majority of the stickers are nonactive. Consequently, not all nonactive stickers are necessarily available for bonding, most probably due to the chain connectivity or the formation of intrachain associations with neighboring stickers. It seems that the three curves in Figure 8a belong to different regions of a common master plot as they follow a logical trend. A master plot is therefore built by shifting the curves according to their maximum number of network junctions, and the results are shown in Figure 8b. The obtained curve shows that for this specific system, the maximum fraction of active stickers is about 60% for a network with N_{max} around 30.

In the same way, the fraction of collective assemblies among active stickers increases sharply for the weakly entangled system, while the growth rate is lowered in the presence of entanglements, as shown in Figure 8c. At the same time, entanglements provide a higher initial fraction of collective assemblies. To put it simply, the slow dynamics and topological constraining of the entanglements increase the probability that a

DOI: 10.1021/acs.macromol.9b00323
Macromolecules 2019, 52, 5255−5267

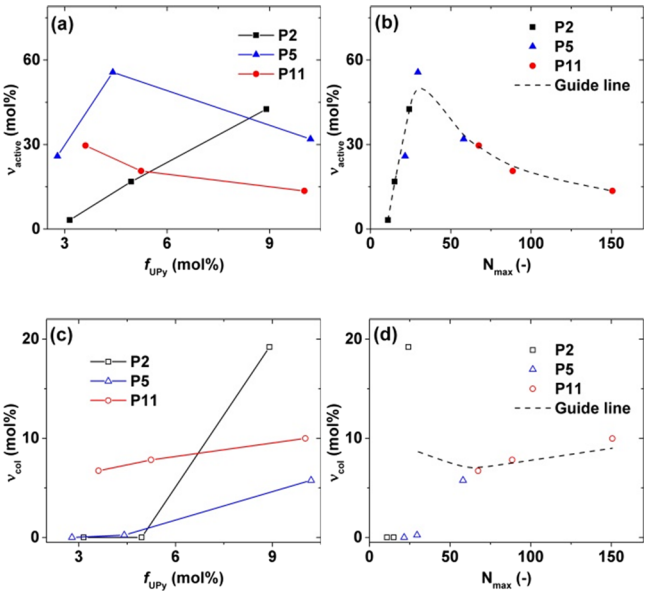

Figure 8. (a, b) Fraction of total active stickers and (c, d) the fraction of collective assemblies as a function of (a, c) UPy content and (b, d) the maximum number of network junctions, N_{max}.

sticker forms a collective assembly. The master plot obtained by shifting the curves according to their N_{max}, as depicted in Figure 8d, demonstrates that the fraction of collective assemblies approaches to a steady value at higher network junctions. This constant value, which of course depends on the relative association affinity of the supramolecular groups, happens to reach about 10% for $N_{max} > 80$ in this study.

V. CONCLUSIONS

Supramolecular polymer networks are frequently idealized by short polymeric precursors physically cross-linked through transient reversible bonds, viewed to be independent binary associations. However, in practice, such an ideal picture is rarely met due to entanglement of long polymeric precursor chains and due to collective assembly of their supramolecular associative groups and by the interplay of these effects. To deconvolute the contributions of these different structural features on the mechanical spectra of supramolecular polymer networks, we have used a well-defined model system to systematically investigate the mutual interplay of the chain length and associative group content and to quantify it in the light of a tube-based model. Thermorheological complexity at high frequencies discloses the presence of free dangling ends, which is the essential source of relaxation in this region. Moreover, the relaxation of the supramolecular polymer chains is explained by contour length fluctuations that are slowed down by a global retraction penalty induced by the stickers. Using the obtained model parameters, we decoupled the contribution of binary associations from those of collective assemblies. This reveals that by increasing the number of network junctions, formed by both stickers and entanglements, the fraction of active stickers and the density of collective ones increase initially, but then, the former decreases steadily, while the latter reaches a constant value. This means that the fraction of active stickers and collective ones can be simply adjusted for unentangled systems; however, chain entanglement limits both parameters to an extent that depends on the association affinity of the utilized supramolecular associative groups. This fundamental understanding of the mutual interplay of chain entanglement and supramolecular dynamics can help in the development of entangled supramolecular polymer network systems with desired short- and long-term mechanical properties.

■ ASSOCIATED CONTENT

Supporting Information

The Supporting Information is available free of charge on the ACS Publications website at DOI: 10.1021/acs.macromol.9b00323.

Supplementary FTIR results and predictions of the stochastic sticky Rouse model (PDF)

■ AUTHOR INFORMATION

Corresponding Authors

*E-mail: mo.ahmadi@aut.ac.ir (M.A.).
*E-mail:evelyne.vanruymbeke@uclouvain.be (E.V.R.).
*E-mail: sebastian.seiffert@uni-mainz.de (S.S.).

ORCID

Mostafa Ahmadi: 0000-0001-6652-4067
Evelyne van Ruymbeke: 0000-0001-7633-0194
Sebastian Seiffert: 0000-0002-5152-1207

Notes

The authors declare no competing financial interest.

■ ACKNOWLEDGMENTS

This work has been supported by a visiting doctorate grant for A.J. of the Graduate School of Excellence "Material Science in Mainz" (MAINZ). M.A. is a Georg Forster fellow of the Alexander von Humboldt Foundation and gratefully acknowledges this support. E.V.R is Chercheuse Qualifiee of the Fond National de la Recherche Scientifique (F.N.R.S.). The authors sincerely thank the reviewers of this paper for their extensive, constructive comments in the process of peer review.

■ REFERENCES

(1) Aida, T.; Meijer, E. W.; Stupp, S. I. Functional supramolecular polymers. *Science* **2012**, *335*, 813−817.
(2) Seiffert, S.; Sprakel, J. Physical chemistry of supramolecular polymer networks. *Chem. Soc. Rev.* **2012**, *41*, 909−930.
(3) Yang, Y.; Urban, M. W. Self-healing polymeric materials. *Chem. Soc. Rev.* **2013**, *42*, 7446−7467.
(4) Yan, X.; Wang, F.; Zheng, B.; Huang, F. Stimuli-responsive supramolecular polymeric materials. *Chem. Soc. Rev.* **2012**, *41*, 6042−6065.
(5) Ji, X.; Yao, Y.; Li, J.; Yan, X.; Huang, F. A supramolecular cross-linked conjugated polymer network for multiple fluorescent sensing. *J. Am. Chem. Soc.* **2012**, *135*, 74−77.
(6) Yoon, H.-J.; Jang, W.-D. Polymeric supramolecular systems for drug delivery. *J. Mater. Chem.* **2010**, *20*, 211−222.
(7) Jangizehi, A.; Ghaffarian, S. R.; Schmolke, W.; Seiffert, S. Dominance of Chain Entanglement over Transient Sticking on Chain Dynamics in Hydrogen-Bonded Supramolecular Polymer Networks in the Melt. *Macromolecules* **2018**, *51*, 2859−2871.
(8) Ahmadi, M.; Hawke, L. G. D.; Goldansaz, H.; Van Ruymbeke, E. Dynamics of entangled linear supramolecular chains with sticky side groups: Influence of hindered fluctuations. *Macromolecules* **2015**, *48*, 7300−7310.
(9) Zhang, Z.; Chen, Q.; Colby, R. H. Dynamics of associative polymers. *Soft Matter* **2018**, *14*, 2961−2977.
(10) Shivokhin, M. E.; Narita, T.; Talini, L.; Habicht, A.; Seiffert, S.; Indei, T.; Schieber, J. D. Interplay of entanglement and association effects on the dynamics of semidilute solutions of multisticker polymer chains. *J. Rheol.* **2017**, *61*, 1231−1241.

DOI: 10.1021/acs.macromol.9b00323
Macromolecules 2019, 52, 5255−5267

(11) Appel, W. P. J.; Portale, G.; Wisse, E.; Dankers, P. Y. W.; Meijer, E. W. Aggregation of ureido-pyrimidinone supramolecular thermoplastic elastomers into nanofibers: a kinetic analysis. *Macromolecules* **2011**, *44*, 6776−6784.
(12) Chen, Q.; Tudryn, G. J.; Colby, R. H. Ionomer dynamics and the sticky Rouse model. *J. Rheol.* **2013**, *57*, 1441−1462.
(13) Chen, S.; Binder, W. H. Dynamic ordering and phase segregation in hydrogen-bonded polymers. *Acc. Chem. Res.* **2016**, *49*, 1409−1420.
(14) Ahmadi, M.; Bailly, C.; Keunings, R.; Nekoomanesh, M.; Arabi, H.; Van Ruymbeke, E. Time marching algorithm for predicting the linear rheology of monodisperse comb polymer melts. *Macromolecules* **2011**, *44*, 647−659.
(15) Van Ruymbeke, E.; Bailly, C.; Keunings, R.; Vlassopoulos, D. A general methodology to predict the linear rheology of branched polymers. *Macromolecules* **2006**, *39*, 6248−6259.
(16) Van Ruymbeke, E.; Keunings, R.; Bailly, C. Prediction of linear viscoelastic properties for polydisperse mixtures of entangled star and linear polymers: Modified tube-based model and comparison with experimental results. *J. Non-Newtonian Fluid Mech.* **2005**, *128*, 7−22.
(17) Read, D. J. From reactor to rheology in industrial polymers. *J. Polym. Sci., Part B: Polym. Phys.* **2015**, *53*, 123−141.
(18) Read, D. J.; Auhl, D.; Das, C.; Den Doelder, J.; Kapnistos, M.; Vittorias, I.; McLeish, T. C. B. Linking models of polymerization and dynamics to predict branched polymer structure and flow. *Science* **2011**, *333*, 1871−1874.
(19) Van Ruymbeke, E.; Lee, H.; Chang, T.; Nikopoulou, A.; Hadjichristidis, N.; Snijkers, F.; Vlassopoulos, D. Molecular rheology of branched polymers: decoding and exploring the role of architectural dispersity through a synergy of anionic synthesis, interaction chromatography, rheometry and modeling. *Soft Matter* **2014**, *10*, 4762−4777.
(20) Hutchings, L. R.; Kimani, S. M.; Hoyle, D. M.; Read, D. J.; Das, C.; McLeish, T. C. B.; Chang, T.; Lee, H.; Auhl, D. In silico molecular design, synthesis, characterization, and rheology of dendritically branched polymers: closing the design loop. *ACS Macro Lett.* **2012**, *1*, 404−408.
(21) Snijkers, F.; Van Ruymbeke, E.; Kim, P.; Lee, H.; Nikopoulou, A.; Chang, T.; Hadjichristidis, N.; Pathak, J.; Vlassopoulos, D. Architectural dispersity in model branched polymers: Analysis and rheological consequences. *Macromolecules* **2011**, *44*, 8631−8643.
(22) Ahmadi, M.; Pioge, S.; Fustin, C.-A.; Gohy, J.-F.; Van Ruymbeke, E. Closer insight into the structure of moderate to densely branched comb polymers by combining modelling and linear rheological measurements. *Soft Matter* **2017**, *13*, 1063−1073.
(23) Entezam, M.; Abbasi, M.; Ahmadi, M. Theoretical correlation of linear and non-linear rheological symptoms of long-chain branching in polyethylenes irradiated by electron beam at relatively low doses. *Rheol. Acta* **2017**, *56*, 729−742.
(24) Cates, M. E. Reptation of living polymers: dynamics of entangled polymers in the presence of reversible chain-scission reactions. *Macromolecules* **1987**, *20*, 2289−2296.
(25) Rubinstein, M.; Semenov, A. N. Dynamics of entangled solutions of associating polymers. *Macromolecules* **2001**, *34*, 1058−1068.
(26) Likhtman, A. E.; McLeish, T. C. B. Quantitative theory for linear dynamics of linear entangled polymers. *Macromolecules* **2002**, *35*, 6332−6343.
(27) Zhuge, F.; Hawke, L. G. D.; Fustin, C.-A.; Gohy, J.-F.; Van Ruymbeke, E. Decoding the linear viscoelastic properties of model telechelic metallo-supramolecular polymers. *J. Rheol.* **2017**, *61*, 1245−1262.
(28) Goldansaz, H.; Voleppe, Q.; Piogé, S.; Fustin, C.-A.; Gohy, J.-F.; Brassinne, J.; Auhl, D.; Van Ruymbeke, E. Controlling the melt rheology of linear entangled metallo-supramolecular polymers. *Soft Matter* **2015**, *11*, 762−774.
(29) Van Ruymbeke, E.; Orfanou, K.; Kapnistos, M.; Iatrou, H.; Pitsikalis, M.; Hadjichristidis, N.; Lohse, D. J.; Vlassopoulos, D. Entangled dendritic polymers and beyond: Rheology of symmetric Cayley-tree polymers and macromolecular self-assemblies. *Macromolecules* **2007**, *40*, 5941−5952.
(30) Van Ruymbeke, E.; Vlassopoulos, D.; Mierzwa, M.; Pakula, T.; Charalabidis, D.; Pitsikalis, M.; Hadjichristidis, N. Rheology and structure of entangled telechelic linear and star polyisoprene melts. *Macromolecules* **2010**, *43*, 4401−4411.
(31) Cui, G.; Boudara, V. A. H.; Huang, Q.; Baeza, G. P.; Wilson, A. J.; Hassager, O.; Read, D. J.; Mattsson, J. Linear shear and nonlinear extensional rheology of unentangled supramolecular side-chain polymers. *J. Rheol.* **2018**, *62*, 1155−1174.
(32) Feldman, K. E.; Kade, M. J.; Meijer, E. W.; Hawker, C. J.; Kramer, E. J. Model transient networks from strongly hydrogen-bonded polymers. *Macromolecules* **2009**, *42*, 9072−9081.
(33) Shabbir, A.; Javakhishvili, I.; Cerveny, S.; Hvilsted, S.; Skov, A. L.; Hassager, O.; Alvarez, N. J. Linear viscoelastic and dielectric relaxation response of unentangled UPy-based supramolecular networks. *Macromolecules* **2016**, *49*, 3899−3910.
(34) Semenov, A. N.; Rubinstein, M. Dynamics of entangled associating polymers with large aggregates. *Macromolecules* **2002**, *35*, 4821−4837.
(35) Indei, T.; Takimoto, J.-i. Linear viscoelastic properties of transient networks formed by associating polymers with multiple stickers. *J. Chem. Phys.* **2010**, *133*, 194902.
(36) Hawke, L. G. D.; Ahmadi, M.; Goldansaz, H.; Van Ruymbeke, E. Viscoelastic properties of linear associating poly (n-butyl acrylate) chains. *J. Rheol.* **2016**, *60*, 297−310.
(37) Jangizehi, A.; Ghaffarian, S. R.; Ahmadi, M. Dynamics of entangled supramolecular polymer networks in presence of high-order associations of strong hydrogen bonding groups. *Polym. Adv. Technol.* **2018**, *29*, 726−735.
(38) Goldansaz, H.; Fustin, C.-A.; Wübbenhorst, M.; Van Ruymbeke, E. How supramolecular assemblies control dynamics of associative polymers: Toward a general picture. *Macromolecules* **2016**, *49*, 1890−1902.
(39) Jangizehi, A.; Ahmadi, M.; Seiffert, S. Dynamics of Supramolecular Associative Polymer Networks at the Interplay of Chain Entanglement, Transient Chain Association, and Chain-Sticker Clustering. *J. Polym. Sci., Part B: Polym. Phys.* **2019**, DOI: 10.1002/polb.24782.
(40) Wang, Z.; Chen, X.; Larson, R. G. Comparing tube models for predicting the linear rheology of branched polymer melts. *J. Rheol.* **2010**, *54*, 223−260.
(41) Chen, Q.; Liang, S.; Shiau, H.-s.; Colby, R. H. Linear viscoelastic and dielectric properties of phosphonium siloxane ionomers. *ACS Macro Lett.* **2013**, *2*, 970−974.
(42) Lewis, C. L.; Stewart, K.; Anthamatten, M. The influence of hydrogen bonding side-groups on viscoelastic behavior of linear and network polymers. *Macromolecules* **2014**, *47*, 729−740.
(43) Gold, B. J.; Hövelmann, C. H.; Lühmann, N.; Pyckhout-Hintzen, W.; Wischnewski, A.; Richter, D. The microscopic origin of the rheology in supramolecular entangled polymer networks. *J. Rheol.* **2017**, *61*, 1211−1226.
(44) Chen, Q.; Zhang, Z.; Colby, R. H. Viscoelasticity of entangled random polystyrene ionomers. *J. Rheol.* **2016**, *60*, 1031−1040.
(45) Zhuge, F.; Hawke, L. G. D.; Fustin, C.-A.; Gohy, J.-F.; Van Ruymbeke, E.; Gold, B.; Colby, R.; Brassinne, J.; Kumar, S.; Rubinstein, M.; Read, D.; Coppola, S.; Watanabe, H.; Louhichi, A. Discussion of paper by F. Zhuge, L. G. D. Hawke, C.-A. Fustin, J.-F. Gohy and E. van Ruymbeke, entitled 'Decoding the linear viscoelastic properties of model telechelic metallo-supramolecular polymers'. *J. Rheol.* **2017**, *61*, 1263−1265.
(46) Amin, D.; Likhtman, A. E.; Wang, Z. Dynamics in supramolecular polymer networks formed by associating telechelic chains. *Macromolecules* **2016**, *49*, 7510−7524.
(47) Van Ruymbeke, E.; Masubuchi, Y.; Watanabe, H. Effective value of the dynamic dilution exponent in bidisperse linear polymers: From 1 to 4/3. *Macromolecules* **2012**, *45*, 2085−2098.
(48) Goldansaz, H.; Jangizehi, A.; Nikravan, G.; Verkinderen, O.; Goderis, B.; Ghaffarian, S. R.; Van Ruymbeke, E.; Ahmadi, M. Rheological Modifiers Based on Supramolecular Block Copolymers:

DOI: 10.1021/acs.macromol.9b00323
Macromolecules 2019, 52, 5255−5267

From Weak Associations to Interconnected Micelles. *React. Funct. Polym.* **2019**, *137*, 27−37.
(49) Van Beek, D. J. M.; Spiering, A. J. H.; Peters, G. W. M.; Te Nijenhuis, K.; Sijbesma, R. P. Unidirectional dimerization and stacking of ureidopyrimidinone end groups in polycaprolactone supramolecular polymers. *Macromolecules* **2007**, *40*, 8464−8475.
(50) Wietor, J.-L.; Van Beek, D. J. M.; Peters, G. W.; Mendes, E.; Sijbesma, R. P. Effects of branching and crystallization on rheology of polycaprolactone supramolecular polymers with ureidopyrimidinone end groups. *Macromolecules* **2011**, *44*, 1211−1219.
(51) Van Gurp, M.; Palmen, J. Time-temperature superposition for polymeric blends. *Rheol. Bull* **1998**, *67*, 5−8.
(52) Tang, S.; Olsen, B. D. Relaxation Processes in Supramolecular Metallogels Based on Histidine−Nickel Coordination Bonds. *Macromolecules* **2016**, *49*, 9163−9175.
(53) Tang, S.; Wang, M.; Olsen, B. D. Anomalous Self-Diffusion and Sticky Rouse Dynamics in Associative Protein Hydrogels. *J. Am. Chem. Soc.* **2015**, *137*, 3946−3957.

DOI: 10.1021/acs.macromol.9b00323
Macromolecules 2019, 52, 5255−5267